 doi:10.20944/preprints202106.0256.v1

Article

Disrupting Mitochondrial Electron Transfer Chain Complex I Decreases Immune Checkpoints in Murine and Human Acute Myeloid Leukemic Cells

Raquel Luna-Yolba [1,2,3,4], Justine Marmoiton [1], Véronique Gigo [1], Xavier Marechal [1], Emeline Boet [2,3,4], Ambrine Sahal [2,3,4], Nathalie Alet[1], Ifat Abramovich[5], Eyal Gottlieb[5], Virgile Visentin[1], Michael R. Paillasse[1],*, Jean-Emmanuel Sarry[2,3,4,6,*]

[1] EVOTEC, Campus Curie, Toulouse, France; Raquel.Luna-Yolba@evotec.com; Justine.Marmoiton@evotec.com; Veronique.Gigo@evotec.com; Xavier.Marechal@evotec.com; Natalie.Alet@evotec.com; Virgile.Visentin@evotec.com; Michael.Paillasse@evotec.com
[2] Centre de Recherches en Cancérologie de Toulouse, Université de Toulouse, Inserm, CNRS, Toulouse, France; emeline.boet@inserm.fr; ambrine.sahal@inserm.fr, jean-emmanuel.sarry@inserm.fr
[3] LabEx Toucan, Toulouse, France
[4] Equipe Labellisée Ligue Nationale Contre le Cancer 2018, Toulouse, France
[5] Technion-Israel Institute of Technology, Haifa, Israel; ifat.a@technion.ac.il ;e.gottlieb@technion.ac.il
[6] Centre Hospitalier Universitaire de Toulouse, Toulouse, France
* Correspondence: michael.paillasse@evotec.com; jean-emmanuel.sarry@inserm.fr; Tel.: (+33)534 63 23-28 (MRP).(+33) 582 74 16 32 (JES)

Simple Summary: Despite all the advancements made in the recent years in the treatment of Acute Myeloid Leukemia (AML), long-term survival are achieved by only 30-40% of AML patients. Thus, new therapeutic strategies are strongly needed. This work confirms the increased in oxidative phosphorylation upon AraC resistance in AML murine cells, reinforcing the interest of targeting it. In addition, it identifies a new role of the first complex of electron transport chain (ETCI) in the regulation of the immune checkpoints PD-L1 and CD39 in murine and human leukemic cells. Thus, this work opens the door to the eventual evaluation of ETCI inhibitors in combination with immunotherapy.

Abstract: Oxidative metabolism is crucial for leukemic stem cell (LSC) function and drug resistance in acute myeloid leukemia (AML). Mitochondrial metabolism also affects the immune system and therefore the antitumor response. Modulation of oxidative phosphorylation (OxPHOS) has emerged as a promising approach to improve therapy outcome for AML patients. However, the effect of mitochondrial inhibitors on the immune compartment in the context of AML is yet to be explored. Immune checkpoints such as the ecto-nucleotidase CD39 and programmed dead ligand 1 (PD-L1) have been reported to be expressed in AML and linked to chemoresistance and poor prognosis. In the present study, we first demonstrated that a novel selective electron transfer chain complex (ETC) I inhibitor, EVT-701, decreased OxPHOS metabolism of murine and human cytarabine (AraC)-resistant leukemic cell lines. Furthermore, we showed that, while AraC induced immune response regulation by increasing CD39 expression and by reinforcing interferon-γ/PD-L1 axis, EVT-701 reduced CD39 and PD-L1 expression in vitro in a panel of both murine and human AML cell lines, especially upon AraC treatment. Altogether, this work uncovers a non-canonical function of ETCI in controlling CD39 and PD-L1 immune checkpoints, thereby improving the anti-tumor response in AML.

Keywords: OxPHOS 1; Immune-checkpoints 2; AML 3.

 doi:10.20944/preprints202106.0256.v1

1. Introduction

Overall survival in acute myeloid leukemia (AML) patients is poor due to relapse after a usually successful induction therapy [1]. This is due to residual leukemic cells after chemotherapy, which regrow resulting in relapse [2]. Energy metabolism and redox homeostasis have emerged as hallmarks of carcinogenesis and their role in the response to chemotherapy in cancer cells is now fully acknowledged [3, 4]. A large body of evidence links both cancer cell stemness and chemotherapy resistance to OxPHOS metabolism [5-9], rendering OxPHOS inhibitors important therapeutic agents to disrupt tumorigenesis and improve chemotherapy outcome. Mitochondrial metabolism has been shown to be a promising target to overcome relapse in leukemia. Recent research has shown that mitochondria in AML cells surviving after chemotherapy have a higher transmembrane potential [10, 11]. In B-progenitor acute lymphoblastic leukemia (B-ALL) diagnosis Relapse Initiating clones (dRI) transcriptionally enriched for mitochondrial metabolism are present from diagnosis [12]. In addition, direct or indirect inhibition of the electron transport chain (ETC)[13- 15] or oxidation of substrates like fatty acids [16] have proven therapeutic benefit in leukemia, synergizing with AraC or with BCL-2 inhibition [17, 18]. One much less studied aspect is the effect of OxPHOS inhibitors in an immunocompetent context, especially in AML, since the vast majority of the studies use NSG mice to allow the study of human cell lines or samples. In other cancer types, metformin has been demonstrated to decrease expression of immune checkpoints components such as PD-L1 [19], CD39 and CD73 [20] both in cancer and immunosuppressive cell populations, enabling CD8 T cell cytotoxic response [19, 21]. However, due to the pleiotropic effects of metformin, it is not clear if these effects are predominately mediated by ETCI inhibition. EVT-701 is a novel ETCI inhibitor that has shown efficacy in different solid tumor models, but its effect on AML has not previously been evaluated [22, 23].

In this study, we report that murine leukemic AML cell lines exposed to AraC behave similar to chemo-resistant human AML cells by upregulating OxPHOS to escape chemotherapy, making our murine model translational to the human pathology. We also show that AraC increased PD-L1 and CD39 immune checkpoint expression at the cell surface membrane. Interestingly, the inhibition of ETCI complex by EVT-701 decreased levels of both immune checkpoints in vitro. Altogether, our findings show that disrupting mitochondrial metabolism through inhibition of ETCI modulates immune checkpoints PD-L1 and CD39 and may improve anti-tumor response in AML.

2. Materials and Methods

Cell culture. Leukemic cell lines were maintained in DMEM medium containing 1g/L of glucose, 2mM glutamax (#35050-038), 1X NEAA (#11140-035, Gibco), 1mM Sodium Pyruvate (#11360-039), all acquired from ThermoFisher Scientific (Illkirch Graffenstaden, France), and 10% Fetal Bovine Serum (#F7524, Sigma-Aldrich, Saint Quentin Fallavier, France). Cells were incubated at 37 °C with 5% CO2 and split every 3 days to maintain exponential growth phase. Cells were purchased from American Type Culture Collection (Rockville, MD, USA). Table 1 summarizes the clinical and mutational features of the leukemic cell lines used in this study.

Preprints (www.preprints.org) | NOT PEER-REVIEWED | Posted: 9 June 2021 doi:10.20944/preprints202106.0256.v1

Table 1. Clinical and mutational information about the AML cell lines used in this study.

	FAB	Karyotype	Sex	FLT3		NPM1	IDH1, IDH2	Kit	N/K Ras
				ITD	TKD				
Murine									
C1498	M5-AML	Normal	F	WT	WT	WT	WT	WT	WT
L1210	B-ALL	Complex	F	WT	WT	WT	WT	WT	WT
Human									
MOLM13	M5-AML	ins(11;9)(q23;p22p23)	M	**ITD**	WT	WT	WT	WT	WT
MV4-11	M5-AML	Complex	M	**ITD**	WT	WT	WT	WT	WT
THP-1	M5-AML	Complex	M	WT	WT	WT	WT	WT	NRAS p.G12D
U937	M5-AML	t(10;11)(p13;q14)	M	WT	WT	WT	WT	WT	WT

IncuCyte assay. Cells were seeded in triplicates in 384-well ViewPlates (#6007480, Perking Elmer, Villebon sur Yvette, France) at a density of 1000 cells/well. After an overnight, cells were stimulated with the compounds and placed into the IncuCyte Zoom (Ozyme, Saint-Cyr-l'Ecole, France) reader until the end of the experiment (5 days after). Images were taken every 3 hours. Confluence for each condition was analyzed using the masks of the IncuCyte Zoom software.

TMRE and MTDR assay. Cells were seeded in fresh media 24h prior to FACs experiments. To prepare the samples, cells were washed in PBS and stained to detect live cells with violet live dead staining (#L34955, ThermoFisher). Then, TetraMethylRhodamine, Ethyl Ester (TMRE) (#T669, Thermo Fisher Scientific) was added for the characterization of the mitochondrial membrane potential and Mitotracker Deep Red FM (#M22426, Thermo Fisher Scientific) was used for the assessment of mitochondrial mass. After incubation at 37 °C for 20 min, cells were washed, resuspended in FACs buffer and analyzed in a FACs Canto (BD Biosciences, Le Pont De Claix, France). FCCP (Sigma-Aldrich) was added as control for specific mitochondrial membrane potential staining.

ATP content assay. ATP cell content was measured using Cell Titer Glo (#G7571, Promega, Charbonnières Les Bains,France). In summary, cells were seeded at 2000 cells/well in 3 replicates in 384-well ViewPlates (Perking Elmer). After an overnight oligomycin A (Sigma-Aldrich) and sodium iodoacetate (Sigma-Aldrich) were added, both either or in combination. Following 1h incubation, cell confluence was assessed with IncuCyte for further normalization, and 40 µL of Cell Titer Glo reaction mix were added to each well, reaching a final volume of 80 µL. Plates were then analyzed for luminescence with EnVision 2105 Multimode Plate Reader (Perkin Elmer). By comparing the different conditions, global ATP and percentages of both glycolytic and mitochondrial ATP were determined.

Cell proliferation. Cell proliferation was calculated by measuring the number of viable cells with trypan blue dye and Nexcelom Bioscience CellometerTM Auto T4 (Ozyme) or staining the cells with live fixable staining (#L34955, ThermoFisher Scientific) and adding counting beads (#C36950, ThermoFisher Scientific) for further analysis with BD LSR Fortessa™ cell analyzer and FlowJo software.

Seahorse. Cells were incubated overnight with vehicle or with EVT-701. Following the incubation time, cells were suspended in pre-warmed Seahorse XF media (Agilent, Les Ulis, France) containing 10 mM glucose, 2 mM glutamine and 1mM pyruvate. 105 cells were seeded per well of Seahorse 96-well plates, previously coated with Cell-tak

Preprints (www.preprints.org) | NOT PEER-REVIEWED | Posted: 9 June 2021 doi:10.20944/preprints202106.0256.v1

(#10317081, ThermoFisher Scientific). The mitostress test was performed with 1-3 µM oligomycin, 1-10 µM FCCP (both optimized for each cell line), 50 µM antimycin/rotenone, and 50 mM 2-DG. OCR and ECAR values were normalized to cell confluence percentage with IncuCyte.
To assess restoration of oxygen consumption by succinate in EVT-treated cells, 10^5 cells were seeded per well in replicates of five. After plate centrifugation, Seahorse media was replaced by pre-warmed Mitochondria Assay Solution (MAS) medium containing 10 mM pyruvate, 4 mM ADP and 2 mM malate, prepared as described by Agilent (https://www.agilent.com/cs/library/usermanuals/public/insert-xf-pmp-reagent-web.pdf). 10 mM Succinate was added to the wells where bypass of ETCI blockade was assessed. Plasma membrane permeabilizer (PMP, Agilent) was added just before the introduction of the plates into the Seahorse reader. Otherwise mentioned, all reagents were bought from Sigma-Aldrich.

Western blot. Cells were lysed with RIPAS buffer (#98065, Cell Signaling Technology, Ozyme) containing protease inhibitor cocktail (#5872S, Cell Signaling Technology, Ozyme). Proteins were quantified by the Pierce BCA protein assay kit (#23227, ThermoFisher Scientific), and protein concentration for each sample was adjusted to 500 µg/mL by adding loading buffer containing DTT, β-mercaptoethanol. Once reduced, samples were heated to 55 °C to complete protein denaturalization without affecting the thermosensitive band of the SDHB (ETCII). Samples were resolved in 4–20% Criterion™ TGX™ Precast Midi Protein Gels from Biorad (#5671093, Marnes-la-Coquette, France) by electrophoresis, transferred to nitrocellulose membranes, and incubated with rodent OxPHOS antibody cocktail (#ab110413) from Abcam (Amsterdam, Netherlands) used at dilution 1:250 or actin (#A2228, Sigma-Aldrich) diluted 1:20 000. Then, incubation with the secondary antibody Goat Anti-Mouse IgG-HRP (#7076, Cell signaling Technology, Ozyme) or Anti-rabbit IgG, HRP-linked Antibody (#7074, Cell signaling) and further addition of Super Signal West Pico Chemiluminescent Substrate (#34580, ThermoFisher Scientific) revealed the protein bands in the membranes. Images were captured with Syngene PXi and quantified with GeneTools from Syngene (ThermoFisher Scientific).

Data sets and Gene Set Enrichment Analysis (GSEA). All publicly accessible transcriptomic data sets used in this study are listed below:

TCGA: [24]
GSE12417: [25]
GSE97631: [10]
MOLM14 treated with metformin: GSE97346

GSEA was performed using DESEQ2 and fGSEA R packages. Gene sets were downloaded from GSEA website (https://www.gsea-msigdb.org/gsea/msigdb/), and the Farge_High OxPHOS signature from [10]. Volcano plots and enrichment maps were used for visualization of the GSEA results. For each gene signature, its Normalized Enrichment Score (NES) and False discovery rate (FDR) considering the p-adjusted values (padj) were evaluated.

Metabolomics. 4 replicates of $7x10^5$ cells/mL were seeded in 6 well plates per experiment. Cells were stimulated with EVT-701 or vehicle. After a 24h incubation with the compounds, 10µL of media were sampled for metabolic extraction, while the remaining media was discarded and cells were washed with PBS. Metabolite extractions were performed by adding 1 mL of cold extraction mix consisting of methanol (#1060351000, Sigma-Aldrich), acetonitrile (#1000291000, Sigma-Aldrich), and water (#1153331000, Sigma-Aldrich) in a proportion 5:3:2. All solvents were LC-MS grade. Samples were vortexed for 10 minutes at 4 °C, and right after centrifuged at maximum speed for 10 minutes at 4 °C. Clear supernatants were transferred to Eppendorf tubes and kept at -80 °C until shipping to the Technion- Israel Institute of Technology for LC-MS analysis. LC-MS metabolomics analysis was performed as described previously (Mackay et al., 2015).

 doi:10.20944/preprints202106.0256.v1

Briefly, Thermo Ultimate 3000 high-performance liquid chromatography (HPLC) system coupled to Q-Exactive Orbitrap Mass Spectrometer (Thermo Fisher Scientific) was used with a resolution of 35,000 at 200 mass/charge ratio (m/z), electrospray ionization, and polarity switching mode to enable both positive and negative ions across a mass range of 67 to 1,000 m/z. HPLC setup consisted ZIC-pHILIC column (SeQuant; 150 mm x 2.1 mm, 5 µm; Merck), with a ZIC-pHILIC guard column (SeQuant; 20 mm x 2.1 mm). 5 µL of the metabolite extracts were injected and the compounds were separated with mobile phase gradient of 15 min, starting at 20% aqueous (20 mM ammonium carbonate adjusted to pH 0.2 with 0.1% of 25% ammonium hydroxide) and 80% organic (acetonitrile) and terminated with 20% acetonitrile. Flow rate and column temperature were maintained at 0.2 ml/min and 45 °C, respectively, for a total run time of 27 min. All metabolites were detected using mass accuracy below 5 ppm. Thermo Xcalibur was used for data acquisition. Analyses were performed with TraceFinder 4.1 (Thermo Fisher Scientific). Peak areas of metabolites were determined by using the exact mass of the singly charged ions. The retention time of metabolites was predetermined on the pHILIC column by analyzing an in-house mass spectrometry metabolite library that was built by running commercially available standards. Cell number was used for data normalization.

Transcriptomics. Cells were seeded in 20 µL at a density of 7500 cells/well in 384-well plates (#3542, Corning, Boulogne-Billancourt, France) and treated with different doses and combination AraC (#PHR1787,Sigma-Aldrich), EVT-701 and IACS or DMSO for 24 h. After a 24 h incubation, plates were centrifuged, and media was replaced by lysis buffer containing RNasin® ribonuclease inhibitor (#2511, Promega). Plates with lysates were frozen to -80 °C and sent to EVOTEC Gottingen, where RNAseq was performed with an in-house library. Data analysis was performed with PanHunter (EVOTEC platform), DESEQ2 and fGSEA R packages.

NAD+/NADH ratio assessment. NAD+/NADH ratio was evaluated using NAD/NADH Glo (#G9072, Promega). In summary, $4x10^5$ cells/mL were seeded in 96-well plates (Perking Elmer) and stimulated with different doses of EVT-701 in a final volume of 200 µL/well. After the 24 h incubation time, NAD+/NADH was evaluated as described (https://france.promega.com/-/media/files/resources/protocols/technical-manuals/101/nad-nadh-glo-assay-protocol.pdf?la=en). Briefly, twice-serial 2-fold dilution of the cells were performed, before diluting another 2 fold with 1% DTAB to lyse the cells. From each well, 50 µL were transferred to a microtube for NAD+ detection in acidic media (25 µL of 0.4N HCl were added) or to an empty tube for NADH detection in basic media. Samples were heated at 60 °C for 15 min, then left 10 min at room temperature. 25 µL of Trizma base were added to the acidic NAD+ sample to neutralize HCl. 50 µL of Trizma-HCl were added to the basic samples containing NADH. From each tube, 4 replicates of 20 µL were seeded in 384-well plates (Perking Elmer). NAD/NADH detection reagent was prepared just before its addition to the well, in ratio 1:1 (20 µL/well). After the incubation time (30-40 min) at room temperature, luminescence was read by using EnVision 2105 Multimode Plate Reader (Perkin Elmer).

PD-L1 and CD39 expression assessment. Murine AML cell lines were seeded in fresh media 72 h prior to the FACs experiment, and stimulated with murine IFN-γ (#575306, BioLegend, Ozyme), EVT-701, AraC, or a combination of the compounds. For human AML cell lines, cells were seeded in fresh media 24 h prior to the FACs experiment, and stimulated with human IFN-γ (#285-IF/CF, R&D Systems, Bio-Techne SAS, Noyal Châtillon sur Seiche, France), EVT-701, AraC, or a combination of the compounds. Then, cells were washed in PBS and stained with violet live dead staining (#L34955, ThermoFisher). Samples were next incubated for 30 min at 4 °C with the correspondent CD39 and PD-L1 antibody mix or the control isotypes, further detailed in table 2. Then, cells were washed and resuspended in FACs buffer, followed by analysis on BD LSRFortessa™ (murine AML cell lines) or BD FACSCanto™ (human AML cell lines) cytometers and

Preprints (www.preprints.org) | NOT PEER-REVIEWED | Posted: 9 June 2021 doi:10.20944/preprints202106.0256.v1

FlowJo software. For NAD supplementation experiments, 0.5 mg/mL NAD+ (#1.24542.0005, Merk) at pH 7 was used. Median fluorescence intensity for each experiment is represented.

Table 2. CD39 and PD-L1 antibodies used in this study.

Antibody	Dilution	Supplier	Catalogue number
anti-mPD-L1-APC	1:50	Biolegend, Ozyme	#BLE124312
APC-anti-Rat IgG2b,κ	1:50	Biolegend, Ozyme	#BLE400611
anti-mCD39-PE-Cy7	1:50	Biolegend, Ozyme	#BLE143806
PE/Cyanine7-anti-Rat IgG2a,κ	1:50	Biolegend, Ozyme	#BLE400522
anti-hPD-L1-APC	1:100	Biolegend, Ozyme	#BLE329708
APC-anti-Mouse IgG2b,κ	1:100	Biolegend, Ozyme	#BLE400320
anti-hCD39-PE-Cy7	1:100	Biolegend, Ozyme	#BLE328212
PE/Cyanine7-anti-Mouse IgG1,κ	1:100	Biolegend, Ozyme	#BLE400126

Statistical analyses. GraphPad Prism Software version 8 (La Jolla, California, USA, www.graphpad.com) was used for the statistical analysis. Results are expressed as mean ± SD. T-test were used for comparison of two groups, whereas one way Anova with Tukey post-test was carried to compare one variant in >2 groups, or two way Anova was used to compare more than 1 variant in >2 groups. Significance is represented by stars in which * is $p<0.05$ ** is $p<0.01$ and *** is $p<0.005$.

Graphical summaries. Graphical schemes were generated using scientific illustration toolkits from motifolio (Motifolio Inc., PO Box 2040, Ellicott City, MD 21041, USA, https://www.motifolio.com/).

3. Results

3.1. OxPHOS phenotype and mitochondrial gene signatures are enriched in AML patients with shorter survival.

The publically available human AML data sets TCGA-AML [24] and Metzeler [25] cohort were analyzed to assess whether there was an association between mitochondrial and OxPHOS gene expression with overall survival. Briefly, each cohort was divided into short or long overall survival (OS > or < to 1 year for both cohorts; Figure 1a-b) and a gene set enrichment analysis (GSEA) was performed. In both cohorts, OxPHOS- and mitochondrial metabolism- related gene signatures were enriched in the short overall survival groups of patients (Figure 1a-b). In addition, sets of genes involved in unfolded protein response and mitochondrial stress were also enriched in short survival patients from the TCGA cohort. Interestingly, higher expression of OxPHOS and NADH-dehydrogenase ETCI complex-related gene signatures derived from AML patients [10] was also seen in shorter survival groups of both TCGA and Metzeler cohorts (Figure 1c), suggesting an involvement of ETCI and mitochondrial metabolism as adverse prognosticators for AML patients.

Preprints (www.preprints.org) | NOT PEER-REVIEWED | Posted: 9 June 2021 doi:10.20944/preprints202106.0256.v1

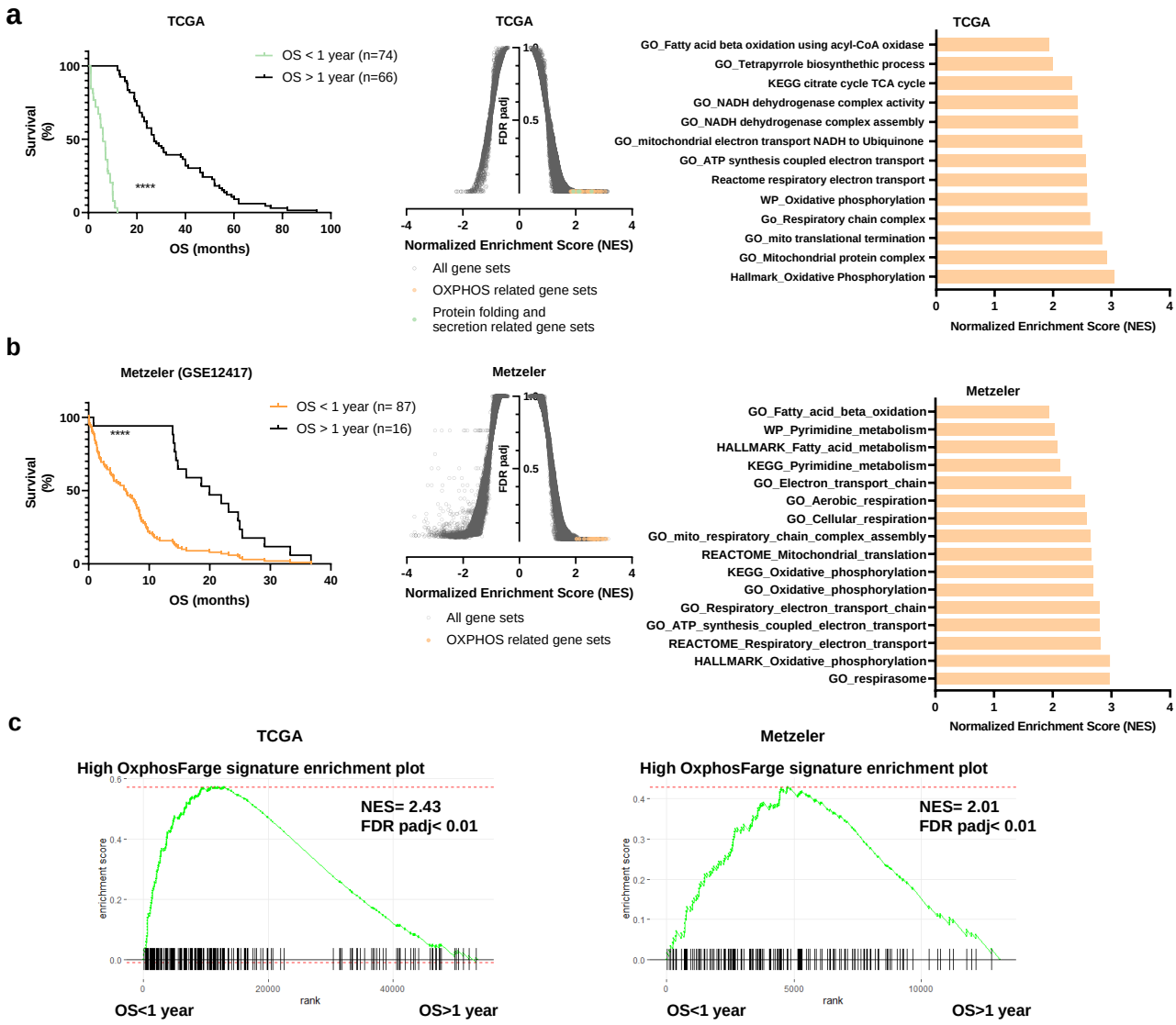

Figure continues on the next page

Preprints (www.preprints.org) | NOT PEER-REVIEWED | Posted: 9 June 2021 doi:10.20944/preprints202106.0256.v1

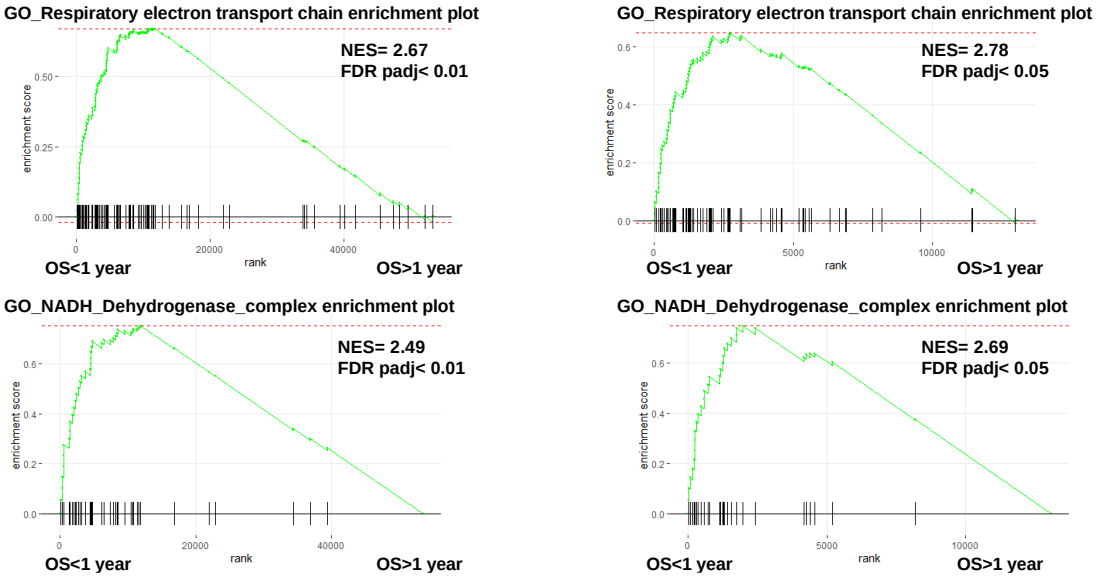

Figure 1. OxPHOS and mitochondrial gene expression is associated with a shorter overall survival in human AML. (**a**) Kaplan Meier survival curves of the TCGA-AML cohort for patients with short (OS > 1 year) or long (OS < 1 year) overall survival (left). Volcano plot showing GSEA results in the TCGA cohort comparing short vs long survival (middle). OxPHOS related gene sets enriched in the short survival group (FDR< 0.01) are highlighted in orange and protein folding and secretion related gene sets (green). On the right, a plot showing TCGA short vs long survival OxPHOS-related differentially expressed gene sets (FDR< 0.05) with their normalized enrichment scores (NES); (**b**) On the left, Kaplan Meier survival curves of the Metzeler cohort for patients with short (OS > 1 year) or long (OS < 1 year) overall survival. In the middle, the volcano plot showing GSEA results in the Metzeler cohort comparing short vs long survival. OxPHOS and mitochondria related gene sets enriched in the short vs long survival group (FDR<0.05) are highlighted in orange. On the right, a plot showing short vs long survival OxPHOS and mitochondria related differentially expressed gene sets (FDR< 0.05) with their normalized enrichment scores (NES); (**c**) Gene set enrichment plots of the Farge-High OxPHOS gene signature, the GO_respiratory electron transport chain and NADH dehydrogenase complex gene signatures in TCGA (left) and in Metzeler (right) cohorts.

3.2. AraC-tolerant murine leukemic cells exhibit a high OxPHOS phenotype also seen in drug resistant human AML cells.

Because we were interested in an immunocompetent context, we assessed whether the previously described high OxPHOS phenotype of AraC-resistant human cells was also observed in murine AML cells. To this end, C1498 and L1210 murine AML cell lines were grown in the presence of AraC (Figure 2a). AraC tolerant cells (C1498-R, L1210-R) displayed higher basal and maximal respiratory rates, as well as higher mitochondrial membrane potential, mass and ATP levels compared to AraC-sensitive cells (C1498-S, L1210-S; Figure 2b-e). Western blots revealed higher expression of ETC complex subunits, especially ETCI, in C1498-R resistant cells compared to C1498-S cells (Figure 2f). In addition, AraC resistant C1498 cells also showed an enrichment in OxPHOS-related gene sets including the high OxPHOS gene signature (Figure 2g-h). Therefore, murine leukemic cells able to grow in the presence of AraC exhibit increased OxPHOS metabolism observed in chemo-resistant human leukemic cells.

Preprints (www.preprints.org) | NOT PEER-REVIEWED | Posted: 9 June 2021 doi:10.20944/preprints202106.0256.v1

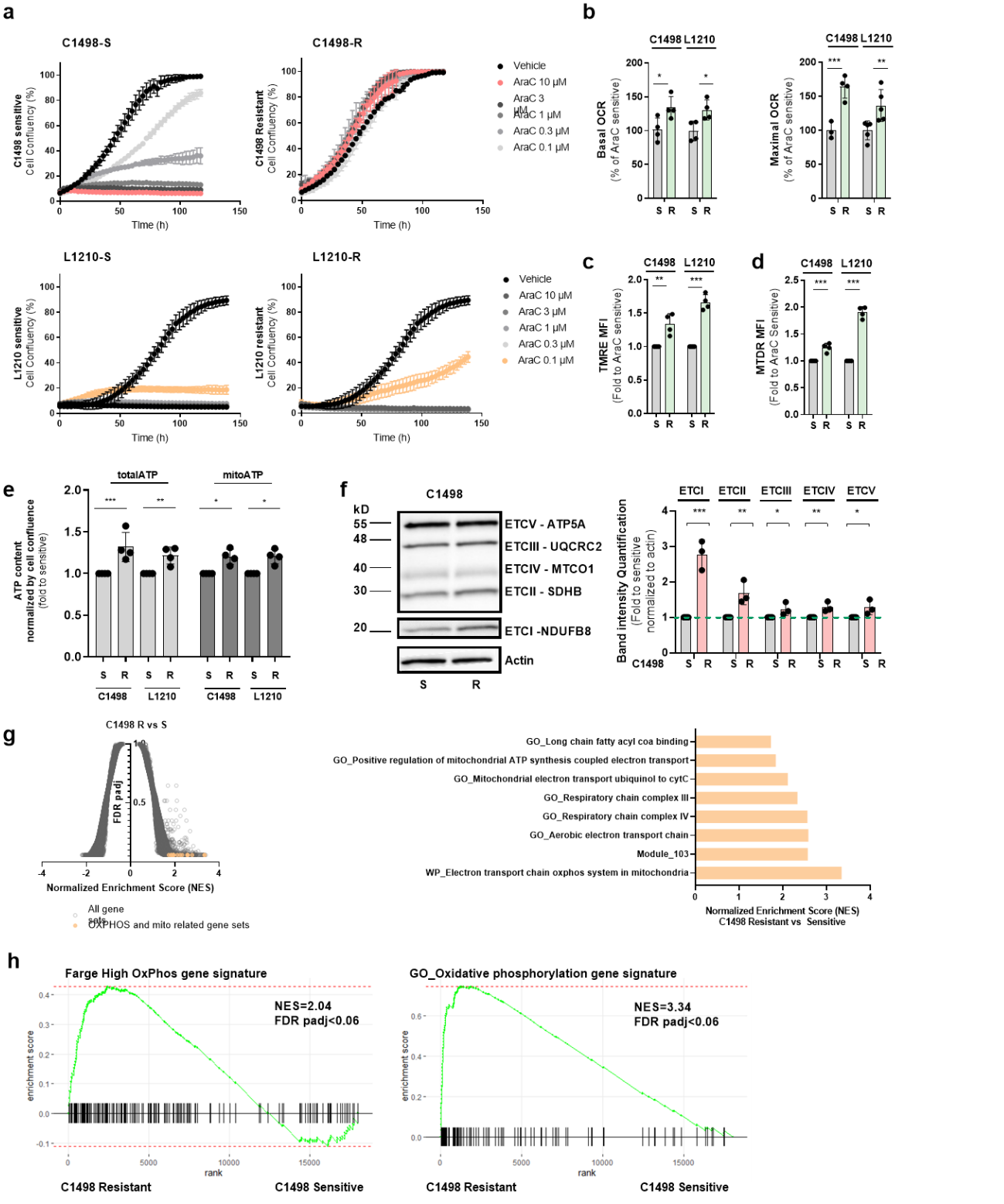

Figure 2. AraC tolerant leukemic cells have more active mitochondria. (**a**) Proliferation IncuCyte assay of murine leukemic C1498 and L1210 cell lines sensitive and resistant to AraC; (**b**) Seahorse assessment of basal and maximal respiration in murine leukemic cells sensitive or tolerant to AraC (N=4); (**c**) FACs assessment of mitochondrial membrane potential with the TMRE probe in AraC sensitive vs resistant conditions for both cell lines (N=4); (**d**) Mitochondrial mass assessment with MTDR (MitoTracker Deep Red) in both cell lines in the condition of sensitiveness and resistance to AraC (N=4); (**e**) Total and mitochondrial ATP content measured by Cell Titer Glo in C1498 and L1210 cell lines sensitive and resistant (N=4); (**f**) Protein expression levels assessed by Western blot of the ETC complexes in C1498 sensitive and resistant to AraC (N=3); (**g**) Volcano plot showing the signatures enriched in AraC resistant vs sensitive C1498 cells (FDR

Preprints (www.preprints.org) | NOT PEER-REVIEWED | Posted: 9 June 2021 doi:10.20944/preprints202106.0256.v1

q-val< 0.05) on the left, and a plot showing OxPhos and mitochondrial related gene sets differentially expressed in resistant vs sensitive condition with their normalized enrichment scores (NES); (**h**) Gene set enrichment plot of the GO oxidative phosphorylation and Farge_High OxPHOS gene signatures in resistant vs sensitive C1498 cells.

3.3. EVT-701 blocks OxPHOS by inhibiting ETCI and induces metabolic compensatory reprogramming in human and murine AML cells.

As shown in solid tumors (ref. 23), EVT-701 was demonstrated here to inhibit oxygen consumption in both murine and human leukemic cell lines grown in the presence of glucose and pyruvate (Figure 3a-b). The blockade in mitochondrial respiration was bypassed in the presence of succinate which donates electrons at the level of ETC complex II (Figure 3c), denoting that EVT-701 does not inhibit electron transport chain beyond ETCI complex. EVT-701 induced a shift toward a glycolytic phenotype as observed by an increase in glucose consumption and lactate production in the exometabolome of the murine leukemic cells (Figure 3d). At the intracellular level, EVT-701 decreased levels of glucose, UDP-GlcNAc, succinic acid, butyryl-carnitine, serine and aspartate, while it increased intracellular lactate in both C1498 and L1210 cell lines (Figure 3e). EVT-701 decreased cell proliferation as single agent in murine leukemic cells (Figure 3f). Importantly, EVT-701 similarly affected mitochondrial function of four human AML cell lines, decreasing OCR, mitochondrial ATP level and the cellular NAD+/NADH ratio (Figure 3g-i) measured in the presence of glucose and pyruvate while it induced a decrease in cell viability (Figure 3j) and showed additive effect to AraC to decrease viability of human AML cells (Figure 3k).

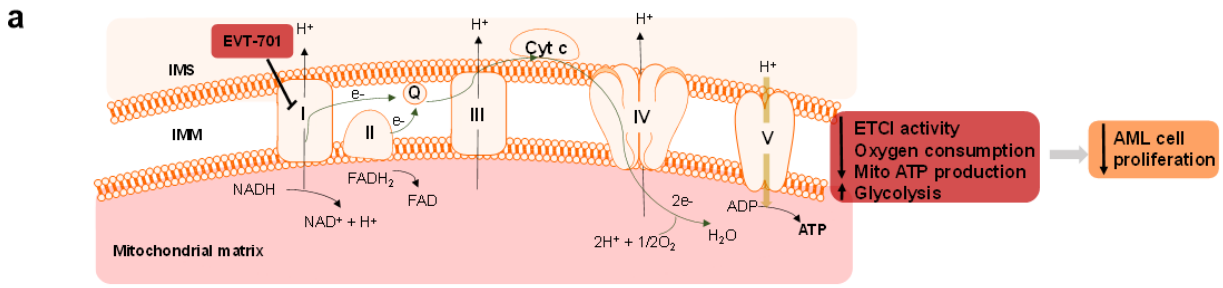

Figure continues on the next page

Figure 3. EVT-701 blocks OxPHOS by inhibiting ETCI and induce a profound metabolic compensatory reprogramming. (**a**) Schematic representation of the mode of action of EVT-701; (**b**) Effect of EVT-701 on basal oxygen consumption rate and ATP production linked to OCR in murine AML cells, assessed by Seahorse (N=4); (**c**) Effect of 10 mM succinate on decrease of oxygen consumption rate induced by EVT-701 in permeabilized leukemic cells (N=4 C1498, N=3 L1201); (**d**) Effect of EVT-701 on lactate and glucose in the exometabolome of C1498 and L1210 after 24h incubation (N=3); (**e**) Effect

Preprints (www.preprints.org) | NOT PEER-REVIEWED | Posted: 9 June 2021 doi:10.20944/preprints202106.0256.v1

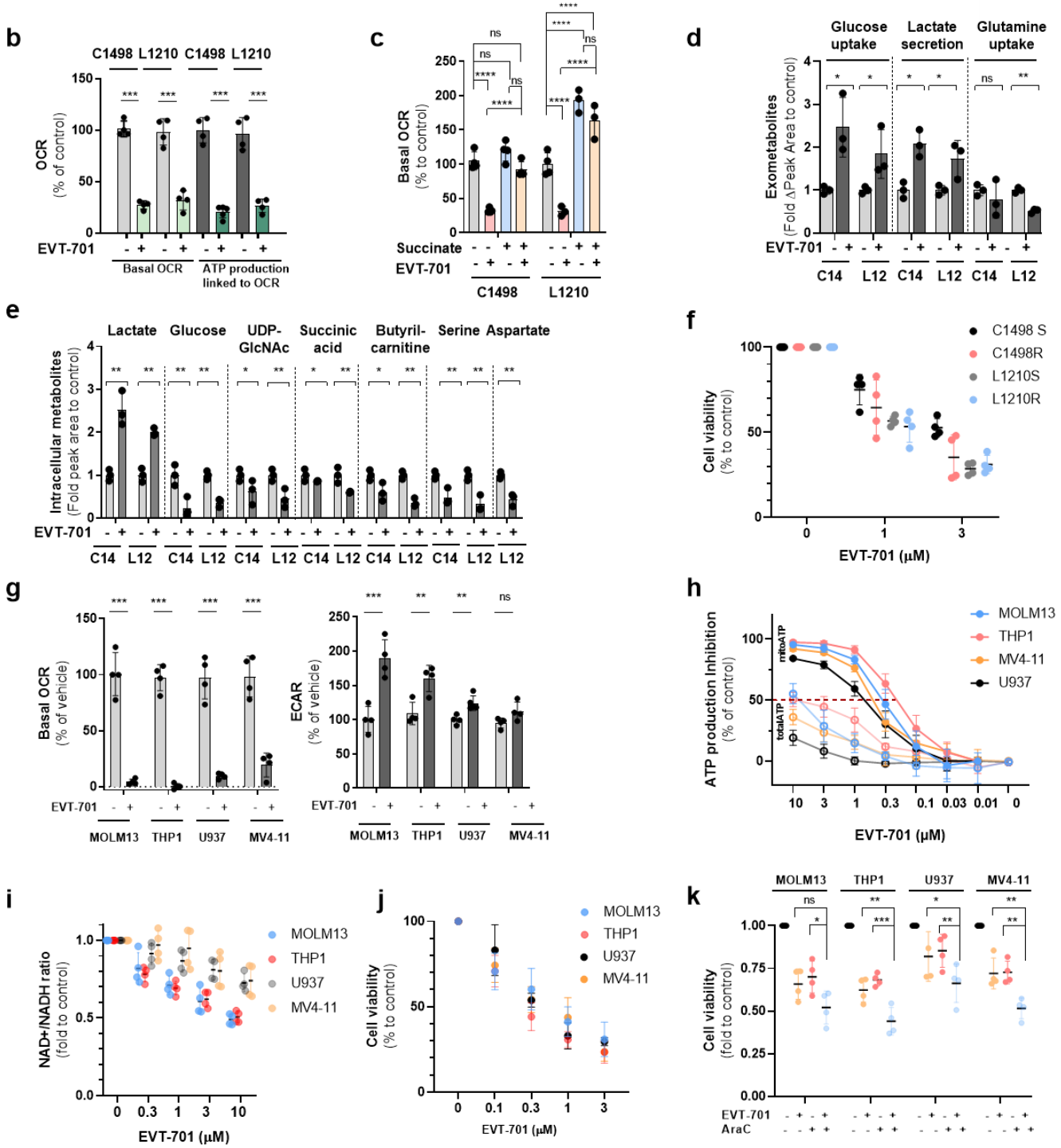

of EVT-701 on intracellular metabolites in C1498 and L1210 cells after 24h incubation (N=3); (**f**) Effect of EVT-701 on C1498 and L1210 proliferation (N=4); (**g**) Effect of EVT-701 on oxygen consumption rate and extracellular acidification rate in human AML cell lines assessed by Seahorse (N=4); (**h**) Dose-response effect of EVT-701 on total ATP and mitochondrial ATP production in human AML cell lines assessed by Cell Titer Glo (N=4); (**i**) NAD+/NADH ratio change in response to EVT-701 in human AML cell lines (N=4). (**j**) Dose response effect of EVT-701 on human AML cell line proliferation (N=4); (**k**) Effect of EVT-701, AraC or their combination on human AML cell line proliferation (N=4).

3.4. EVT-701 decreases expression of immune checkpoint markers in murine and human leukemic cells.

GSEA showed that gene sets associated with interferon-γ response or signaling pathways that lead to increased expression of PD-L1 were enriched in AraC-residual AML cells (Figure 4a) and in patients with the shorter overall survival (OS; Figure 4b-c) indicating a key

Preprints (www.preprints.org) | NOT PEER-REVIEWED | Posted: 9 June 2021 doi:10.20944/preprints202106.0256.v1

role of immune checkpoints in relapse to chemotherapy in AML. Interestingly, the transcriptome of murine resistant cells was enriched in interferon-γ response gene signature as well (Figure 4e). To confirm this observation, we assessed CD39 and inducible PD-L1 levels by flow cytometry in murine and human leukemic cell lines treated with EVT-701, AraC or their combination. AraC increased cell surface expression of both inducible PD-L1 and CD39 in leukemic cells while EVT-701 as single agent as well as in combination with AraC decreased these proteins in the cellular membrane, suggesting potential as an immunomodulatory agent (Figure 4 d-f). Interestingly, ETCI inhibition with IACS also resulted in decreased CD39 and inducible PD-L1 membrane levels (Supplementary figure s1b-c). In addition, CD39 mRNA was also decreased by metformin (Supplementary figure s1d). EVT-701 as single agent and in combination with AraC decreased the cellular NAD+/NADH ratio (Figure 4g), which has recently been proposed as the driving factor of inducible PD-L1 decreased expression (ref. 26). Indeed, media supplementation with NAD+ restored PD-L1 levels in the presence of EVT-701 or IACS, while CD39 levels were not altered by exogenous NAD+ in the presence of ETCI inhibitors (figure 4h-i), showing a differential modulatory effect of ETCI inhibition on the two checkpoints. In addition, while PD-L1 expression was induced by IFN-γ, CD39 was unaffected (Supplementary figure S1a), highlighting a different regulatory mechanism for both immune checkpoints. In sum, EVT-701 may be able to decrease tumor-mediated immunosuppression by decreasing inducible PD-L1 and CD39 expression on leukemic cells.

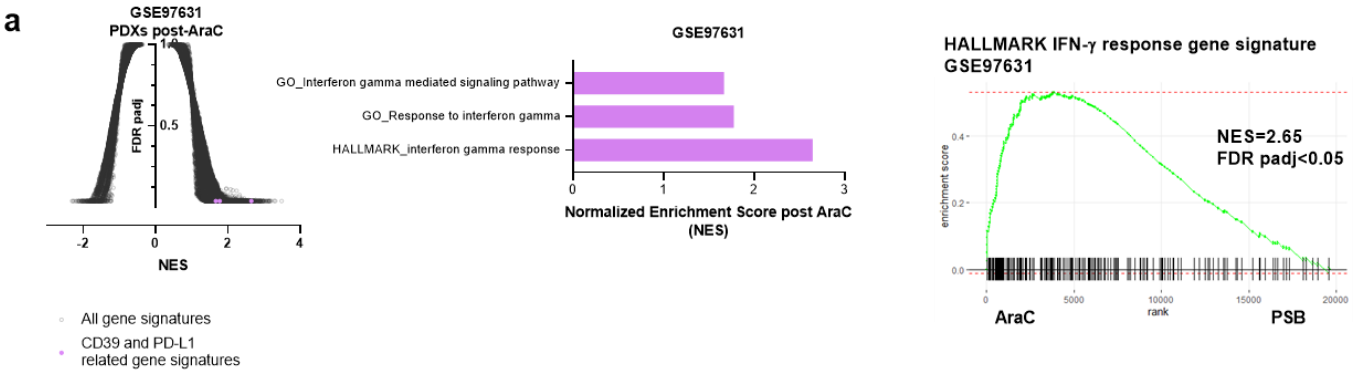

Figure continues on the next page

Preprints (www.preprints.org) | NOT PEER-REVIEWED | Posted: 9 June 2021 doi:10.20944/preprints202106.0256.v1

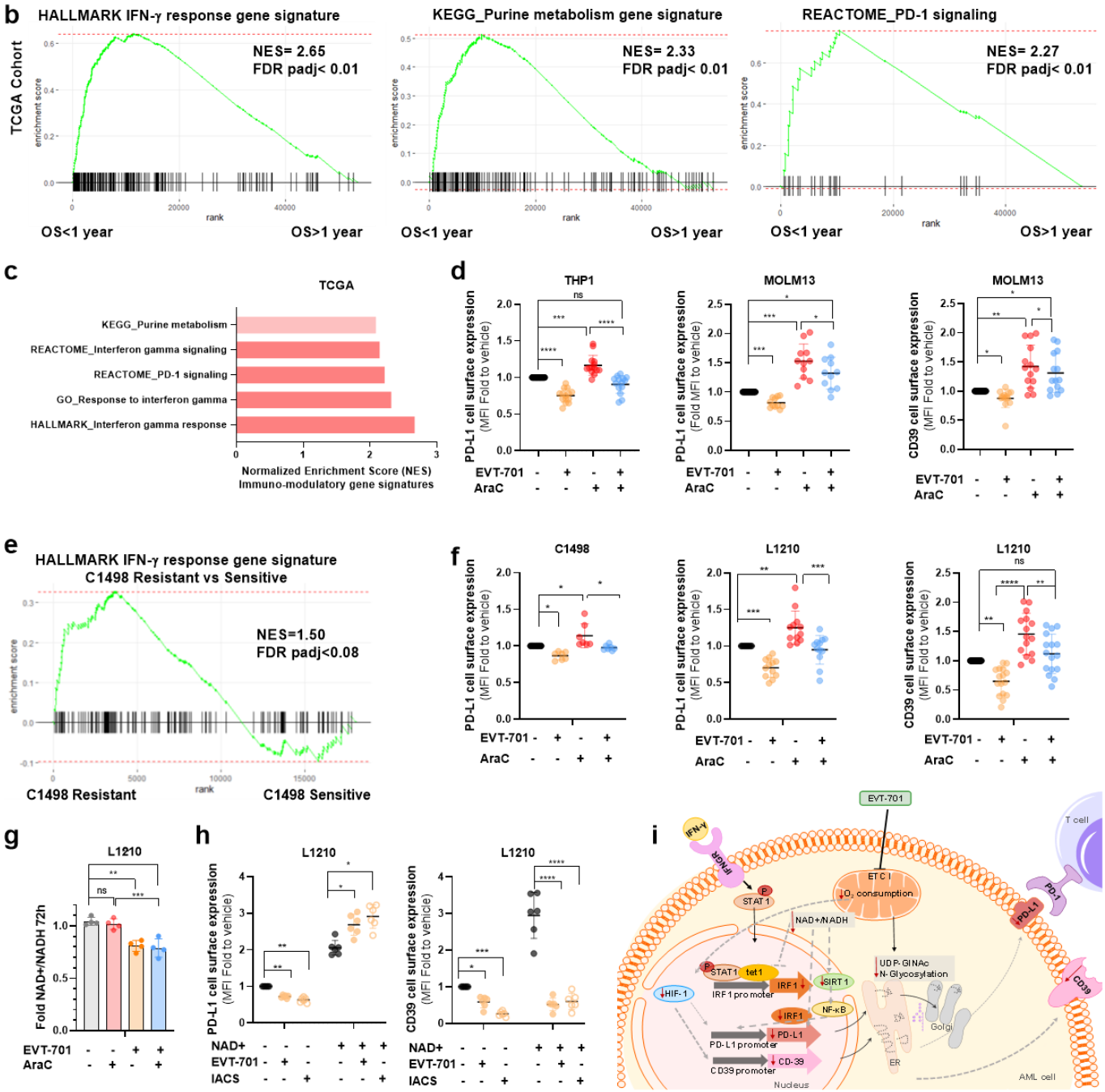

Figure 4. EVT-701 decreases immune checkpoints expression to boost immune response and increase the therapeutic benefit.(**a**) Volcano plot showing GSEA results in the GSE97631 data set, containing the transcriptomic profiles of residual AML in PDXs AraC or vehicle treated. Immune-modulation related gene signatures are in purple. In the middle, a plot showing AraC vs PBS treated PDXs-differentially expressed gene sets with their normalized enrichment scores (NES). On the right, the enrichment plot of the Hallmark_Interferon-γ gene signature, compatible with PD-L1 increase after AraC in vivo; (**b**) Enrichment plots of the Hallmark_Interferon-γ gene signature (left), KEGG_purine metabolism containing CD39 (middle) and Reactome_PD-1 signaling (right) in the short group survival of the TCGA cohort; (**c**) Plot showing CD39 and PD-L1 related signatures in the short group of the TCGA cohort with their normalized enrichment scores (NES); (**d**) FACS assessment of the modulation of inducible PD-L1 and CD39 membrane expression on THP1 and MOLM13 cells by EVT-701, AraC or combination of both (N>10); (**e**) Enrichment plot of the Hallmark_Interferon-γ gene signature in C1498 resistant vs sensitive cells transcriptome; (**f**) FACs assessment of the modulation of inducible and CD39 membrane expression on C1498 (N=7) and L1210 (N>10) by EVT-701, AraC or combination of both at 72h; (**g**) Effect of EVT-701, AraC or combination of both on NAD+/NADH ratio in L1210 at 72h (N=4); (**h**) Effect of exogenous NAD+ on modulation of PD-L1 and CD39 membrane levels by EVT-701 or with IACS (N=6); (**i**) Schematic view of the proposed mechanism of action of EVT-701 as

 doi:10.20944/preprints202106.0256.v1

4. Discussion

In summary, we have demonstrated that the OxPHOS phenotype induced by metabolic adaptation to chemotherapy is a common mechanism in murine and human AML cells and many other forms of cancer [10, 11]. In addition, we have shown that the genetic signatures of shorter survival groups within human AML cohorts are enriched in OxPHOS and mitochondrial metabolism gene sets, underscoring the involvement of mitochondria in progression and relapse of the disease. We characterized the effect of EVT-701, a new selective ETCI inhibitor, on metabolism in human and murine AML cell lines, characterizing the metabolic reprogramming it exerts on AML cells by inducing a shift toward glycolysis, increasing glucose consumption and lactate production while decreasing mitochondrial ATP production and the cellular NAD+/NADH ratio. The metabolic changes observed upon EVT-701 suggest an impairment of OxPHOS function and all have been previously observed with other ETCI inhibitors. Glycolytic shift upon ETCI inhibition (Pasteur effect) has been already observed with other ETCI inhibitors, such as metformin [27]. In addition, a fall in aspartate levels also occurred with IACS-01759 (hereafter IACS)[15]. This is explained by the drop in NAD+/NADH ratio induced by ETCI inhibition, that impairs aspartate biosynthesis by interfering with mitochondrial malate dehydrogenase (MDH2) activity [28, 29]. It has been also reported in several works that de novo serine biosynthesis is impaired upon ETCI inhibition [30, 31], while being still catabolized via folate pathway [31], leading to the reduction in serine levels. The decrease in succinic acid could suggest decreased TCA activity though the levels of other TCA cycle intermediates were not consistently reduced in this study. This could be compatible with TCA replenishment through glutamine-derived reductive carboxylation of α-KG via NADPH-dependent isocitrate dehydrogenase 1 (IDH1) to generate citrate, what has also been observed with other ETCI inhibitors [32, 33], despite EVT-701 does not stimulate glutamine uptake (figure 3d). In addition, EVT-701 decreased proliferation of AML cells both as a single agent and in combination with AraC. Using in vitro models, we showed that AraC increased CD39 and inducible PD-L1 at cell surface, while EVT-701 as single agent decreased expression levels of these proteins and, when used in combination with AraC, neutralized the increase induced by the chemotherapeutic agent. In addition, we showed that the decrease of immune checkpoints is not exclusive to EVT-701, since other ETCI inhibitors, such as IACS and, as reported in literature, metformin elicited similar responses [19, 20].

Because NAD+ supplementation abrogated the decrease of inducible PD-L1 expression but not that of CD39 upon ETCI inhibition and considering as well that only PD-L1 is induced by IFN-γ, we propose that two different regulatory mechanisms concur to achieve modulation of these two immune checkpoint components. It is important to remark that, despite the controversy around the NAD+ uptake by mammalian cells, it has been previously reported that exogenous NAD+ can rescue cells from death upon NAD depletion induced by the nicotinamide phosphoribosyl transferase (NAMPT) inhibitor FK866 [34]. In addition, NAD+ supplementation might also rescue cells from the block in DNA repair resulting from PARP1 inactivation upon FK866 NAD-depletion [35], reinforcing the assumption that NAD+ can be uptaken and used by the cells. Remarkably, MCART1/SLC25A51 has been recently identified as the NAD importer in mitochondria of mammal cells, and to be necessary for ETCI activity [36, 37]. Interestingly, previous studies showed that exogenous NAD+ can access mammalian mitochondria, and increase respiration [38]. Therefore, supplementation with NAD+ could potentially affect intracellular NAD+/NADH ratio changes induced by ETCI inhibition in our cellular context. The proposed regulatory mechanism of PD-L1 involves ETCI-driven NAD+ as a major coordinator. NAD+ is known to be cofactor of sirtuin 1 (SIRT1), a class III histone deacetylase involved in epigenetic control [39]. Resveratrol is a SIRT1 agonist that has been reported to stimulate ETCI activity to increase NAD+/NADH ratio and activate SIRT1 [40]. Inter-

estingly, several studies described that resveratrol upregulated PD-L1 expression in several cancer types including colon, breast and lung cancer [41, 42, 43]. One of these studies supported that PD-L1 expression was upregulated upon SIRT1 activation with resveratrol via NF-κB [42]. Remarkably, PD-L1 inducible expression has been reported to be upregulated through IFN-γ activation of the NF-κB pathway [41]. Interestingly, recent work identifies ETCI function to be essential for IFN-γ signaling, since upon genetic or pharmacological function abrogation of exclusively the first ETC complex, IFN-γ signaling is impaired and PD-L1 levels are decreased [44]. This study suggests that the NAD+ driven by functional ETCI is essential for IFN-γ signaling, since impaired activity of exclusively ETCI is enough to decrease IFN- γ signaling pathway and PD-L1 expression. Interestingly, it's been recently observed that OxPHOS cells have increased PD-L1 levels [45, 46].

In addition, functional ETCI and NAD metabolism have been shown to be involved in the epigenetic regulation of inducible PD-L1 expression [26]. In fact, this study proposed a mechanism by which NAD+ metabolism, via TCA intermediates such α-ketoglutarate (α-KG), activates TET1. TET1 then interacts with p-STAT1, previously phosphorylated and activated by JAK after IFN-γ IFNGR stimulation. They showed that the TET1-p-STAT1 interaction stabilized TET-1 and facilitated TET1-mediated demethylation of Irf1 promoter, what would subsequently promote the generation of IRF1, and induce PD-L1 expression [47, 48, 49]. The link between TET1 activity and PD-L1 expression has already been proposed in glioma. Lower PD-L1 levels have been reported in patients bearing IDH mutations, increasing (R)-2-hydroxyglutarate (2-HG) oncometabolite production [50, 51]. 2-HG is a competitive inhibitor of multiple α-KG dependent dioxygenases, which includes the TET family of 5-methlycytosine hydroxylase [52, 53], thereby explaining the loss of TET activity concomitant with IDH mutations. It has recently been reported that in response to 2-HG inhibition, PD-L1 levels in IDH1 mutant tumors were increased to the same levels observed in WT-IDH gliomas [54]. Since IDH mutations are also present in some AML patients [55, 56], the same profile regarding IDH mutational state and PD-L1 levels might also be expected though this remains to be proven. In addition, TET1 repression has also been associated with increased tumor- infiltrating immune cells in several cancer types, such as basal-like breast cancer (BLBC), melanoma, ovarian, lung and thyroid cancer [57]. Considering all the above mentioned, we propose that ETCI-NADH dehydrogenase activity regulates the level and ratios of NAD+/NADH, that is essential for SIRT1 and/or TET1-mediated PD-L1 stimulation. Recent studies showed that CD39 expression was not induced by IFN-γ [58, 59], whereas it can be induced under hypoxic conditions [60, 61]. ETCI inhibitors have already been reported to interfere with HIF stabilization, such as IACS [15, 62] and metformin [63, 64, 65]. EVT-701 was also developed from a screening campaign to characterize HIF-1α inhibitors [22], therefore we propose an impairment of hypoxic signaling by interfering with HIF-1α stabilization as the mechanism by which EVT-701 decreases CD39 expression. Importantly, EVT-701 was shown to decrease levels of the N-glycosylation unit UDP-GlcNAc, which can impair CD39 function and localization in the cell membrane [66], highlighting another layer of the regulation of CD39 by EVT-701.

5. Conclusions

In conclusion, this work describes the opposed actions of chemotherapy and ETCI inhibitors on immune system modulation, providing a non-canonical function of ETCI in the regulation of CD39 and PD-L1 and a rationale to improve anti-tumor response in AML, including combinations with immune checkpoint therapies.

Supplementary Materials: The following are available online at www.mdpi.com/xxx/s1, Figure S1: Supplemental figure 1; Supplemental material S2: Western blot raw images, Supplemental material S3: densiometry readings of Western blot bands

Author Contributions: RLY, MRP, VV, NA designed the studies and interpreted the data; RLY, JES wrote the manuscript; MRP, VV, JES supervised the work; RLY performed the experiments; XM

contributed to the set-up, design and generation of transcriptomic samples; JM, VG contributed to western blot experiments. EB, AS contributed to technical development and tools. EG, IA supervised and helped analyzing metabolomics studies. All authors approved the submitted version of the manuscript.

Funding: This study has been funded by the European Union's Horizon 2020 Research and Innovation Programme under the Marie Skłodowska-Curie Grant Agreements 766214 (META-CAN). EVT-701 and related compounds were licensed from Sanofi to Evotec in 2015.

Data Availability Statement: GEO accession codes of data sets used in the study are GSE12417; GSE97631; GSE97346, GSEXXXXX (the transcriptomic data C1498 R vs S is currently being submitted to GEO. The definitive accession number will be updated as soon as it will be assigned).

Acknowledgments: We thank all members of Team METAML for their support and technical assistance. The authors also thank Dr Mary Selak for critical reading of the manuscript.

Conflicts of Interest: RLY, JM, VG, NA, VV & MRP are full time employees of Evotec SE. The other authors declare no competing interests.

References

1. Döhner, H.; Weisdorf, D.J.; Bloomfield, C.D. Acute Myeloid Leukemia. *New England Journal of Medicine* **2015**, *373*, 1136–1152, doi:10.1056/nejmra1406184.
2. Yilmaz, M.; Wang, F.; Loghavi, S.; Bueso-Ramos, C.; Gumbs, C.; Little, L.; Song, X.; Zhang, J.; Kadia, T.; Borthakur, G.; et al. Late relapse in acute myeloid leukemia (AML): clonal evolution or therapy-related leukemia? *Blood Cancer Journal* **2019**, *9*, doi:10.1038/s41408-019-0170-3
3. Hanahan, D.; Weinberg, Robert A. Hallmarks of Cancer: The Next Generation. *Cell* **2011**, *144*, 646–674, doi:10.1016/j.cell.2011.02.013.
4. Pavlova, Natalya N.; Thompson, Craig B. The Emerging Hallmarks of Cancer Metabolism. *Cell Metabolism* **2016**, *23*, 27–47, doi:10.1016/j.cmet.2015.12.006.
5. Lonardo, E.; Cioffi, M.; Sancho, P.; Sanchez-Ripoll, Y.; Trabulo, S.M.; Dorado, J.; Balic, A.; Hidalgo, M.; Heeschen, C. Metformin Targets the Metabolic Achilles Heel of Human Pancreatic Cancer Stem Cells. *PLoS ONE* **2013**, *8*, e76518, doi:10.1371/journal.pone.0076518.
6. Vazquez, F.; Lim, J.-H.; Chim, H.; Bhalla, K.; Girnun, G.; Pierce, K.; Clish, Clary B.; Granter, Scott R.; Widlund, Hans R.; Spiegelman, Bruce M.; et al. PGC1α Expression Defines a Subset of Human Melanoma Tumors with Increased Mitochondrial Capacity and Resistance to Oxidative Stress. *Cancer Cell*. **2013**;23:287–301.
7. Ricci J-E, Chiche J. Metabolic Reprogramming of Non-Hodgkin's B-Cell Lymphomas and Potential Therapeutic Strategies. *Frontiers in Oncology* **2018**, *8*, doi:10.3389/fonc.2018.00556.
8. Faubert, B.; Solmonson, A.; DeBerardinis, R.J. Metabolic reprogramming and cancer progression. *Science* **2020**, *368*, eaaw5473, doi:10.1126/science.aaw5473.
9. . Vivas-García, Y.; Falletta, P.; Liebing, J.; Louphrasitthiphol, P.; Feng, Y.; Chauhan, J.; Scott, D.A.; Glodde, N.; Chocarro-Calvo, A.; Bonham, S.; et al. Lineage-Restricted Regulation of SCD and Fatty Acid Saturation by MITF Controls Melanoma Phenotypic Plasticity. *Molecular Cell* **2020**, *77*, 120-137.e9, doi:10.1016/j.molcel.2019.10.014.
10. Farge, T.; Saland, E.; de Toni, F.; Aroua, N.; Hosseini, M.; Perry, R.; Bosc, C.; Sugita, M.; Stuani, L.; Fraisse, M.; et al. Chemotherapy-Resistant Human Acute Myeloid Leukemia Cells Are Not Enriched for Leukemic Stem Cells but Require Oxidative Metabolism. *Cancer Discovery* **2017**, *7*, 716–735, doi:10.1158/2159-8290.cd-16-0441.
11. Kuntz, E.M.; Baquero, P.; Michie, A.M.; Dunn, K.; Tardito, S.; Holyoake, T.L.; Helgason, G.V.; Gottlieb, E. Targeting mitochondrial oxidative phosphorylation eradicates therapy-resistant chronic myeloid leukemia stem cells. *Nature Medicine* **2017**, *23*, 1234–1240, doi:10.1038/nm.4399.
12. Dobson SM, García-Prat L, Vanner RJ, Wintersinger J, Waanders E, Gu Z, McLeod, J.; Gan, O.I.; Grandal, I.; Payne-Turner, D.; et al. Relapse-Fated Latent Diagnosis Subclones in Acute B Lineage Leukemia Are Drug Tolerant and Possess Distinct Metabolic Programs. *Cancer Discovery*. **2020**;10:568–87. doi:10.1158/2159-8290.cd-19-1059.
13. Cole, A.; Wang, Z.; Coyaud, E.; Voisin, V.; Gronda, M.; Jitkova, Y.; Mattson, R.; Hurren, R.; Babovic, S.; Maclean, N.; et al. Inhibition of the Mitochondrial Protease ClpP as a Therapeutic Strategy for Human Acute Myeloid Leukemia. *Cancer Cell* **2015**, *27*, 864–876, doi:10.1016/j.ccell.2015.05.004.
14. . Liyanage, S.U.; Hurren, R.; Voisin, V.; Bridon, G.; Wang, X.; Xu, C.; MacLean, N.; Siriwardena, T.P.; Gronda, M.; Yehudai, D.; et al. Leveraging increased cytoplasmic nucleoside kinase activity to target mtDNA and oxidative phosphorylation in AML. *Blood* **2017**, *129*, 2657–2666, doi:10.1182/blood-2016-10-741207.
15. Molina JR, Sun Y, Protopopova M, Gera S, Bandi M, Bristow C, .; McAfoos, T.; Morlacchi, P.; Ackroyd, J.; Agip, A.-N.A.; et al. An inhibitor of oxidative phosphorylation exploits cancer vulnerability. *Nature Medicine*. **2018**; 24:1036–46, doi:10.1038/s41591-018-0052-4.

16. Samudio, I.; Harmancey, R.; Fiegl, M.; Kantarjian, H.; Konopleva, M.; Korchin, B.; Kaluarachchi, K.; Bornmann, W.; Duvvuri, S.; Taegtmeyer, H.; et al. Pharmacologic inhibition of fatty acid oxidation sensitizes human leukemia cells to apoptosis induction. *Journal of Clinical Investigation* **2010**, *120*, 142–156, doi:10.1172/jci38942.
17. Stuani, L.; Sabatier, M.; Sarry, J.-E. Exploiting metabolic vulnerabilities for personalized therapy in acute myeloid leukemia. *BMC Biology* **2019**, *17*, doi:10.1186/s12915-019-0670-4.
18. Bosc, C.; Gadaud, N.; Bousard, A.; Sabatier, M.; Cognet, G.; Saland, E.; Farge, T.; Boet, E.; Gotanègre, M.; Aroua, N.; et al. Mitochondrial determinants of response and resistance to venetoclax plus cytarabine duplet therapy in acute myeloid leukemia. *bioRxiv* **2020**, doi:10.1101/2020.08.17.253856
19. Cha, J.-H.; Yang, W.-H.; Xia, W.; Wei, Y.; Chan, L.-C.; Lim, S.-O.; Li, C.-W.; Kim, T.; Chang, S.-S.; Lee, H.-H.; et al. Metformin Promotes Antitumor Immunity via Endoplasmic-Reticulum-Associated Degradation of PD-L1. *Molecular Cell* **2018**, *71*, 606-620.e7, doi:10.1016/j.molcel.2018.07.030.
20. Li, L.; Wang, L.; Li, J.; Fan, Z.; Yang, L.; Zhang, Z.; Zhang, C.; Yue, D.; Qin, G.; Zhang, T.; et al. Metformin-Induced Reduction of CD39 and CD73 Blocks Myeloid-Derived Suppressor Cell Activity in Patients with Ovarian Cancer. *Cancer Research* **2018**, *78*, 1779–1791, doi:10.1158/0008-5472.can-17-2460.
21. Pereira, F.V.; Melo, A.C.L.; Low, J.S.; de Castro, Í.A.; Braga, T.T.; Almeida, D.C.; de Lima, A.G.U.B.; Hiyane, M.I.; Correa-Costa, M.; Andrade-Oliveira, V.; et al. Metformin exerts antitumor activity via induction of multiple death pathways in tumor cells and activation of a protective immune response. *Oncotarget* **2018**, *9*, doi:10.18632/oncotarget.25380
22. Méneyrol, J (**2018**). Benzylhydroxyde derivatives, preparation thereof and therapeutic use thereof (U.S. Patent No 9,878,990 B2). U.S. Patent and Trademark Office.
23. Luna-Yolba R, Visentin V, Hervé C, Chiche J, Ricci J-E, Méneyrol J, et al. EVT-701 is a novel selective and safe mitochondrial complex 1 inhibitor with potent anti-tumor activity in models of solid cancers. **2021**. *Submitted for publication*.
24. Cancer Genome Atlas Research Network. Genomic and Epigenomic Landscapes of Adult De Novo Acute Myeloid Leukemia. *New England Journal of Medicine* **2013**, *368*, 2059–2074, doi:10.1056/nejmoa1301689.
25. Metzeler, K.H.; Hummel, M.; Bloomfield, C.D.; Spiekermann, K.; Braess, J.; Sauerland, M.-C.; Heinecke, A.; Radmacher, M.; Marcucci, G.; Whitman, S.P.; et al. An 86-probe-set gene-expression signature predicts survival in cytogenetically normal acute myeloid leukemia. *Blood* **2008**, *112*, 4193–4201, doi:10.1182/blood-2008-02-134411.
26. Lv H, Lv G, Chen C, Zong Q, Jiang G, Ye D; Cui, X.; He, Y.; Xiang, W.; Han, Q.; et al. NAD+ Metabolism Maintains Inducible PD-L1 Expression to Drive Tumor Immune Evasion. *Cell Metabolism*. **2020**;33, doi:10.1016/j.cmet.2020.10.021.
27. Scotland, S.; Saland, E.; Skuli, N.; de Toni, F.; Boutzen, H.; Micklow, E.; Sénégas, I.; Peyraud, R.; Peyriga, L.; Théodoro, F.; et al. Mitochondrial energetic and AKT status mediate metabolic effects and apoptosis of metformin in human leukemic cells. *Leukemia* **2013**, *27*, 2129–2138, doi:10.1038/leu.2013.107.
28. Birsoy, K.; Wang, T.; Chen, Walter W.; Freinkman, E.; Abu-Remaileh, M.; Sabatini, David M. An Essential Role of the Mitochondrial Electron Transport Chain in Cell Proliferation Is to Enable Aspartate Synthesis. *Cell* **2015**, *162*, 540–551, doi:10.1016/j.cell.2015.07.016.
29. Sullivan, Lucas B.; Gui, Dan Y.; Hosios, Aaron M.; Bush, Lauren N.; Freinkman, E.; Vander Heiden, Matthew G. Supporting Aspartate Biosynthesis Is an Essential Function of Respiration in Proliferating Cells. *Cell* **2015**, *162*, 552–563, doi:10.1016/j.cell.2015.07.017.
30. Diehl FF, Lewis CA, Fiske BP, Vander Heiden MG. Cellular redox state constrains serine synthesis and nucleotide production to impact cell proliferation. *Nature Metabolism* **2019**, *1*, 861–867, doi:10.1038/s42255-019-0108-x.
31. Yang, L.; Garcia Canaveras, J.C.; Chen, Z.; Wang, L.; Liang, L.; Jang, C.; Mayr, J.A.; Zhang, Z.; Ghergurovich, J.M.; Zhan, L.; et al. Serine Catabolism Feeds NADH when Respiration Is Impaired. *Cell Metabolism* **2020**, *31*, 809-821.e6, doi:10.1016/j.cmet.2020.02.017.
32. Mullen, A.R.; Wheaton, W.W.; Jin, E.S.; Chen, P.-H.; Sullivan, L.B.; Cheng, T.; Yang, Y.; Linehan, W.M.; Chandel, N.S.; DeBerardinis, R.J. Reductive carboxylation supports growth in tumour cells with defective mitochondria. *Nature* **2011**, *481*, 385–388, doi:10.1038/nature10642.
33. Mullen, A R.; Hu, Z.; Shi, X.; Jiang, L.; Boroughs, Lindsey K.; Kovacs, Z.; Boriack, R.; Rakheja, D.; Sullivan, Lucas B.; Linehan, W. Marston; et al. Oxidation of Alpha-Ketoglutarate Is Required for Reductive Carboxylation in Cancer Cells with Mitochondrial Defects. *Cell Reports* **2014**, *7*, 1679–1690, doi:10.1016/j.celrep.2014.04.037.
34. Billington, R.A.; Travelli, C.; Ercolano, E.; Galli, U.; Roman, C.B.; Grolla, A.A.; Canonico, P.L.; Condorelli, F.; Genazzani, A.A. Characterization of NAD Uptake in Mammalian Cells. *Journal of Biological Chemistry* **2008**, *283*, 6367–6374, doi:10.1074/jbc.M706204200.
35. Wilk, A.; Hayat, F.; Cunningham, R.; Li, J.; Garavaglia, S.; Zamani, L.; Ferraris, D.M.; Sykora, P.; Andrews, J.; Clark, J.; et al. Extracellular NAD+ enhances PARP-dependent DNA repair capacity independently of CD73 activity. *Scientific Reports* **2020**, *10*, doi:10.1038/s41598-020-57506-9.
36. Kory, N.; uit de Bos, J.; van der Rijt, S.; Jankovic, N.; Güra, M.; Arp, N.; Pena, I.A.; Prakash, G.; Chan, S.H.; Kunchok, T.; et al. MCART1/SLC25A51 is required for mitochondrial NAD transport. *Science Advances* **2020**, *6*, eabe5310, doi:10.1126/sciadv.abe5310.
37. Luongo, T.S.; Eller, J.M.; Lu, M.-J.; Niere, M.; Raith, F.; Perry, C.; Bornstein, M.R.; Oliphint, P.; Wang, L.; McReynolds, M.R.; et al. SLC25A51 is a mammalian mitochondrial NAD+ transporter. *Nature* **2020**, *588*, 174–179, doi:10.1038/s41586-020-2741-7.

38. Davila, A.; Liu, L.; Chellappa, K.; Redpath, P.; Nakamaru-Ogiso, E.; Paolella, L.M.; Zhang, Z.; Migaud, M.E.; Rabinowitz, J.D.; Baur, J.A. Nicotinamide adenine dinucleotide is transported into mammalian mitochondria. *eLife* **2018**, *7*, doi:10.7554/elife.33246.
39. Etchegaray, J.-P.; Mostoslavsky, R. Interplay between Metabolism and Epigenetics: A Nuclear Adaptation to Environmental Changes. *Molecular Cell* **2016**, *62*, 695–711, doi:10.1016/j.molcel.2016.05.029.
40. Desquiret-Dumas V, Gueguen N, Leman G, Baron S, Nivet-Antoine V, Chupin S, Chevrollier, A.; Vessières, E.; Ayer, A.; Ferré, M.; et al. Resveratrol Induces a Mitochondrial Complex I-dependent Increase in NADH Oxidation responsible for Sirtuin Activation in Liver Cells. *Journal of Biological Chemistry*. **2013**;288:36662–75, doi:10.1074/jbc.m113.466490.
41. .Gowrishankar, K.; Gunatilake, D.; Gallagher, S.J.; Tiffen, J.; Rizos, H.; Hersey, P. Inducible but Not Constitutive Expression of PD-L1 in Human Melanoma Cells Is Dependent on Activation of NF-κB. *PLOS ONE* **2015**, *10*, e0123410, doi:10.1371/journal.pone.0123410.
42. Lucas, J.; Hsieh, T.-C.; Halicka, H.D.; Darzynkiewicz, Z.; Wu, J. Upregulation of PD-L1 expression by resveratrol and piceatannol in breast and colorectal cancer cells occurs via HDAC3/p300-mediated NF-κB signaling. *International Journal of Oncology* **2018**, doi:10.3892/ijo.2018.4512.
43. Yang, M.; Li, Z.; Tao, J.; Hu, H.; Li, Z.; Zhang, Z.; Cheng, F.; Sun, Y.; Zhang, Y.; Yang, J.; et al. Resveratrol induces PD-L1 expression through snail-driven activation of Wnt pathway in lung cancer cells. *Journal of Cancer Research and Clinical Oncology* **2021**, *147*, 1101–1113, doi:10.1007/s00432-021-03510-z.
44. Kiritsy MC, Mott D, Behar SM, Sassetti CM, Olive AJ. Mitochondrial respiration contributes to the interferon gamma response in antigen presenting cells. *bioRxiv* **2020**, doi:10.1101/2020.11.22.393538.
45. Wangpaichitr M, Kandemir H, Li Y, Wu C, Nguyen D, Feun L, .; Kuo, M.; Savaraj, N. Relationship of Metabolic Alterations and PD-L1 Expression in Cisplatin Resistant Lung Cancer. *Cell & Developmental Biology*. **2017**;06, doi:10.4172/2168-9296.1000183..
46. Valle, S.; Alcalá, S.; Martin-Hijano, L.; Cabezas-Sáinz, P.; Navarro, D.; Muñoz, E.R.; Yuste, L.; Tiwary, K.; Walter, K.; Ruiz-Cañas, L.; et al. Exploiting oxidative phosphorylation to promote the stem and immunoevasive properties of pancreatic cancer stem cells. *Nature Communications* **2020**, *11*, doi:10.1038/s41467-020-18954-z.
47. Garcia-Diaz A, Shin DS, Moreno BH, Saco J, Escuin-Ordinas H, Rodriguez GA, Zaretsky, J.M.; Sun, L.; Hugo, W.; Wang, X.; et al. Interferon Receptor Signaling Pathways Regulating PD-L1 and PD-L2 Expression. *Cell Reports*. **2017**;19:1189–201, doi:10.1016/j.celrep.2017.04.031.
48. Moon, J.W.; Kong, S.-K.; Kim, B.S.; Kim, H.J.; Lim, H.; Noh, K.; Kim, Y.; Choi, J.-W.; Lee, J.-H.; Kim, Y.-S. IFNγ induces PD-L1 overexpression by JAK2/STAT1/IRF-1 signaling in EBV-positive gastric carcinoma. *Scientific Reports* **2017**, *7*, doi:10.1038/s41598-017-18132-0.
49. Yan, Y.; Zheng, L.; Du, Q.; Yan, B.; Geller, D.A. Interferon regulatory factor 1 (IRF-1) and IRF-2 regulate PD-L1 expression in hepatocellular carcinoma (HCC) cells. *Cancer Immunology, Immunotherapy* **2020**, *69*, 1891–1903, doi:10.1007/s00262-020-02586-9.
50. Berghoff, A.S.; Kiesel, B.; Widhalm, G.; Wilhelm, D.; Rajky, O.; Kurscheid, S.; Kresl, P.; Wöhrer, A.; Marosi, C.; Hegi, M.E.; et al. Correlation of immune phenotype with IDH mutation in diffuse glioma. *Neuro-Oncology* **2017**, *19*, 1460–1468, doi:10.1093/neuonc/nox054.
51. Mu, L.; Long, Y.; Yang, C.; Jin, L.; Tao, H.; Ge, H.; Chang, Y.E.; Karachi, A.; Kubilis, P.S.; De Leon, G.; et al. The IDH1 Mutation-Induced Oncometabolite, 2-Hydroxyglutarate, May Affect DNA Methylation and Expression of PD-L1 in Gliomas. *Frontiers in Molecular Neuroscience* **2018**, *11*, doi:10.3389/fnmol.2018.00082. Mu L, Long Y, Yang C, Jin L, Tao H, Ge H, et al. The IDH1 Mutation-Induced Oncometabolite, 2-Hydroxyglutarate, May Affect DNA Methylation and Expression of PD-L1 in Gliomas. Frontiers in Molecular Neuroscience. 2018;11.
52. Figueroa, M.E.; Abdel-Wahab, O.; Lu, C.; Ward, P.S.; Patel, J.; Shih, A.; Li, Y.; Bhagwat, N.; Vasanthakumar, A.; Fernandez, H.F.; et al. Leukemic IDH1 and IDH2 mutations result in a hypermethylation phenotype, disrupt TET2 function, and impair hematopoietic differentiation. *Cancer Cell* **2010**, *18*, 553–567, doi:10.1016/j.ccr.2010.11.015.
53. Xu, W.; Yang, H.; Liu, Y.; Yang, Y.; Wang, P.; Kim, S.-H.; Ito, S.; Yang, C.; Wang, P.; Xiao, M.-T.; et al. Oncometabolite 2-Hydroxyglutarate Is a Competitive Inhibitor of α-Ketoglutarate-Dependent Dioxygenases. *Cancer Cell* **2011**, *19*, 17–30, doi:10.1016/j.ccr.2010.12.014.
54. Kadiyala, P.; Carney, S.V.; Gauss, J.C.; Garcia-Fabiani, M.B.; Haase, S.; Alghamri, M.S.; Núñez, F.J.; Liu, Y.; Yu, M.; Taher, A.; et al. Inhibition of 2-hydroxyglutarate elicits metabolic reprogramming and mutant IDH1 glioma immunity in mice. *Journal of Clinical Investigation* **2021**, *131*, doi:10.1172/jci139542.
55. Mardis, E.R.; Ding, L.; Dooling, D.J.; Larson, D.E.; McLellan, M.D.; Chen, K.; Koboldt, D.C.; Fulton, R.S.; Delehaunty, K.D.; McGrath, S.D.; et al. Recurring Mutations Found by Sequencing an Acute Myeloid Leukemia Genome. *New England Journal of Medicine* **2009**, *361*, 1058–1066, doi:10.1056/nejmoa0903840.
56. Ward, P.S.; Patel, J.; Wise, D.R.; Abdel-Wahab, O.; Bennett, B.D.; Coller, H.A.; Cross, J.R.; Fantin, V.R.; Hedvat, C.V.; Perl, A.E.; et al. The Common Feature of Leukemia-Associated IDH1 and IDH2 Mutations Is a Neomorphic Enzyme Activity Converting α-Ketoglutarate to 2-Hydroxyglutarate. *Cancer Cell* **2010**, *17*, 225–234, doi:10.1016/j.ccr.2010.01.020.
57. Collignon, E.; Canale, A.; Al Wardi, C.; Bizet, M.; Calonne, E.; Dedeurwaerder, S.; Garaud, S.; Naveaux, C.; Barham, W.; Wilson, A.; et al. Immunity drives TET1 regulation in cancer through NF-κB. *Science Advances* **2018**, *4*, eaap7309, doi:10.1126/sciadv.aap7309.
58. Castro, F.; Cardoso, A.P.; Gonçalves, R.M.; Serre, K.; Oliveira, M.J. Interferon-Gamma at the Crossroads of Tumor Immune Surveillance or Evasion. *Frontiers in Immunology* **2018**, *9*, doi:10.3389/fimmu.2018.00847.

59. Jorgovanovic, D.; Song, M.; Wang, L.; Zhang, Y. Roles of IFN-γ in tumor progression and regression: a review. *Biomarker Research* **2020**, *8*, doi:10.1186/s40364-020-00228-x.
60. Eltzschig HK, Ibla JC, Furuta GT, Leonard MO, Jacobson KA, Enjyoji K, Robson, S.C.; Colgan, S.P. Coordinated Adenine Nucleotide Phosphohydrolysis and Nucleoside Signaling in Posthypoxic Endothelium. *Journal of Experimental Medicine*. **2003**;198:783–96, doi:10.1084/jem.20030891.
61. Eltzschig HK, Köhler D, Eckle T, Kong T, Robson SC, Colgan SP. Central role of Sp1-regulated CD39 in hypoxia/ischemia protection. *Blood*. **2009**;113:224–32, doi:10.1182/blood-2008-06-165746.
62. . Rytelewski, M.; Harutyunyan, K.; Baran, N.; Mallampati, S.; Zal, M.A.; Cavazos, A.; Butler, J.M.; Konoplev, S.; El Khatib, M.; Plunkett, S.; et al. Inhibition of Oxidative Phosphorylation Reverses Bone Marrow Hypoxia Visualized in Imageable Syngeneic B-ALL Mouse Model. *Frontiers in Oncology* **2020**, *10*, doi:10.3389/fonc.2020.00991.
63. Zhou, X.; Chen, J.; Yi, G.; Deng, M.; Liu, H.; Liang, M.; Shi, B.; Fu, X.; Chen, Y.; Chen, L.; et al. Metformin suppresses hypoxia-induced stabilization of HIF-1α through reprogramming of oxygen metabolism in hepatocellular carcinoma. *Oncotarget* **2015**, *7*, 873–884, doi:10.18632/oncotarget.6418.
64. Guimarães TA, Farias LC, Santos ES, de Carvalho Fraga CA, Orsini LA, de Freitas Teles L, Feltenberger, J.D.; de Jesus, S.F.; de Souza, M.G.; Sousa Santos, S.H.;et al. Metformin increases PDH and suppresses HIF-1α under hypoxic conditions and induces cell death in oral squamous cell carcinoma. *Oncotarget*. **2016**;7:55057–68, doi:10.18632/oncotarget.10842..
65. Kocemba-Pilarczyk, K.A.; Trojan, S.; Ostrowska, B.; Lasota, M.; Dudzik, P.; Kusior, D.; Kot, M. Influence of metformin on HIF-1 pathway in multiple myeloma. *Pharmacological Reports* **2020**, *72*, 1407–1417, doi:10.1007/s43440-020-00142-x.
66. Zhong X, Malhotra R, Woodruff R, Guidotti G. Mammalian Plasma Membrane Ecto-nucleoside Triphosphate Diphosphohydrolase 1, CD39, Is Not Active IntracellularlyThe N-glycosylation state of CD39 correlates with surface activity and localization. *Journal of Biological Chemistry*. **2001**;276:41518–25, doi:10.1074/jbc.M104415200.